Available online at www.sciencedirect.com
SCIENCE DIRECT®
Optics Communications 215 (2003) 125–134
OPTICS COMMUNICATIONS
www.elsevier.com/locate/optcom

Bifurcation transitions in an optically injected diode laser: theory and experiment

Sebastian Wieczorek [a,*], Thomas B. Simpson [b], Bernd Krauskopf [c], Daan Lenstra [a]

[a] *Faculty of Sciences, Vrije Universiteit Amsterdam, De Boelelaan 1081, 1081 HV Amsterdam, The Netherlands*
[b] *Jaycor/Titan, 3394 Carmel Mountain Road, San Diego, CA 92121, USA*
[c] *Department of Engineering Mathematics, University of Bristol, Bristol BS8 1TR, UK*

Received 13 August 2002; accepted 12 November 2002

Abstract

We show how bifurcation theory and experimental measurements can be used hand-in-hand to analyse transitions to complicated dynamics in a semiconductor laser subject to optical injection. By a direct comparison of theoretical and experimental optical spectra we identify and explain the underlying dynamics in phase space. This is demonstrated with four distinct bifurcation transitions, including a transition near a saddle-node Hopf point and an intermittent transition to chaos.

PACS: 42.50.Ne; 42.55.Px; 05.45.+b

Keywords: Laser with optical injection; Bifurcation diagrams; Bifurcation transitions

1. Introduction

Dynamical systems theory is a powerful tool to explain and even predict complicated dynamics in applications by analysing appropriate mathematical models. What is needed for success is a relatively simple model, for example, in the form of a low-dimensional system of ordinary differential equations (ODEs), that nevertheless captures the essence of an experiment under consideration. Well-known examples are the Lorenz equations and the equations describing what is now called Chua's circuit; see e.g. Ref. [1].

A particularly nice and technologically relevant example is that of a single-mode semiconductor laser receiving optical injection from a stable laser source (also referred to as a master laser). Physically, it is conceptually the most basic semiconductor laser system showing complicated dynamics and chaos; see the overviews [2,3] and references therein. At the same time, the injected laser can be modeled by a set of three ODEs, introduced as Eq. (1) below, that can be derived in an intuitive and rather phenomenological way. It is now well

* Corresponding author. Semiconductor Material Sciences, Sandia National Laboratories, P.O. Box 50800, MS 0601, Albuquerque, NM 87185-0601, USA.
E-mail address: smwiecz@sandia.gov (S. Wieczorek).

0030-4018/02/$ - see front matter
PII: S0030-4018(02)02191-0

established that these equations, in spite of their apparent simplicity, display an astonishing level of agreement with experimental measurements. Fig. 1 shows a direct comparison between the experimentally obtained stability map in the plane of injection strength and detuning of a distributed feedback (DFB) laser and the respective computed bifurcation diagram; see also [4].

The experimental measurements of Fig. 1(a) were performed with a DFB semiconductor laser operating at a wavelength of approximately 1.557 mm, which received unidirectional optical injection from a master laser via a fiber coupling using an optical circulator. The DFB laser maintained single-mode operation throughout the wide parameter range that we considered. Both master and slave laser were under independent current and temperature control. The operational parameters of the experiment are the offset frequency of the master with respect to the free-running DFB laser (in GHz) and injected power (in arbitrary units), which were varied by changing the operating temperature of the master laser and a variable attenuator, respectively. A microwave spectrum analyser was used to obtain optical spectra with a frequency resolution of better than 100 MHz and a dynamic range greater than 50 dB. For more details on the experimental setup and measurement techniques see the experimental companion paper [5].

The experimental stability diagram in Fig. 1(a) was generated by stepping the master laser and recording qualitative changes in the optical spectra of the DFB laser. Diamonds correspond to a transition from four-wave mixing to locked dynamics. The difference between full and open diamonds at negative offset frequencies is due to a bistability discussed in Section 2. Squares denote the onset of the so-called relaxation oscillations, triangles the location of a first and circles that of a second period doubling. Finally, crosses mark transitions to more complicated (possibly chaotic) dynamics.

The bifurcation diagram in Fig. 1(b) was obtained by using numerical continuation to find curves of bifurcations of the well-established rate equation model [6] of a single-mode semiconductor laser subject to optical injection. These rate equations for the complex electric field amplitude $E = E_x + iE_y$ and the population inversion n define a three-dimensional dynamical system. They can be written in dimensionless form as:

$$\begin{aligned} \dot{E} &= K + \left(\frac{1}{2}(1+i\alpha)n - i\omega\right)E, \\ \dot{n} &= -2\Gamma n - (1+2Bn)(|E|^2 - 1) \end{aligned} \tag{1}$$

in the frame of reference of the injected field. To allow for a direct comparison with the experiment, the parameters α, B and Γ in Eq. (1) were set to the

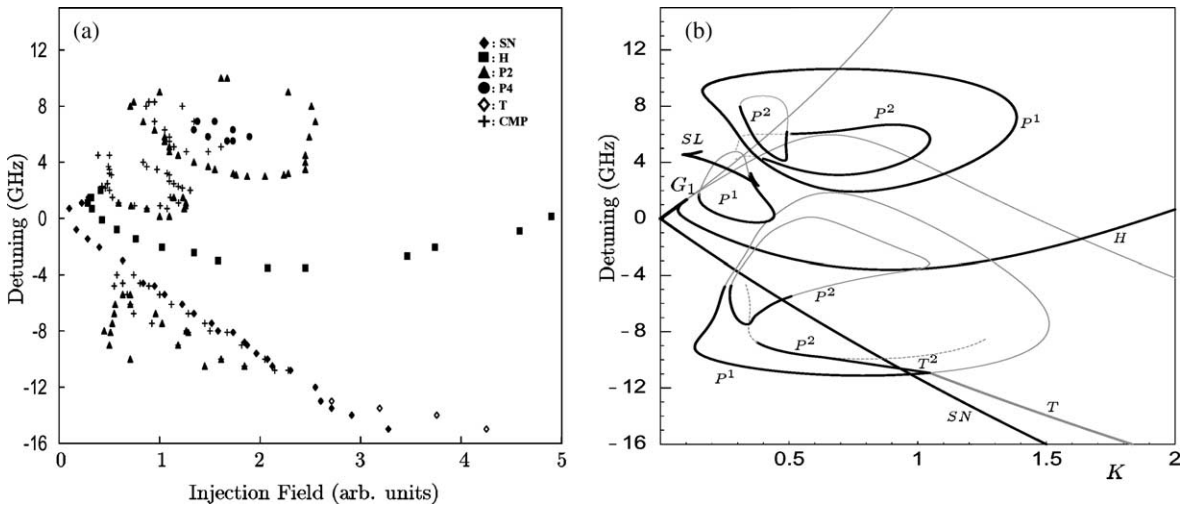

Fig. 1. Experimental stability map (a) and theoretical bifurcation diagram (b).

experimentally determined values $\alpha = 2.6$, $B = 0.0295$ and $\Gamma = 0.0973$. The bifurcation parameters are the injection strength K and the detuning ω. The detuning is plotted in units of GHz and the range of the K-axis was chosen to have the best possible agreement between the locking ranges in Fig. 1(a) and (b). Supercritical bifurcations (of stable solutions) in Fig. 1(a) are plotted as black curves, and they can be compared directly with the measured qualitative changes in Fig. 1(a). The subcritical grey bifurcation curves (of unstable objects) are needed to obtain a consistent bifurcation diagram.

The agreement between the two diagrams in Fig. 1 was discussed in detail in [4]. The goal of the present paper is to focus on certain regions of the bifurcation diagram where interesting transitions of the dynamics occur. We show here that the excellent agreement of the experimental and theoretical parameter diagrams is matched by an equally good agreement on the level of experimental and theoretical optical spectra. This gives much more confidence when interpreting sequences of often ambiguous experimental spectra detailing complicated and/or sudden transitions to chaos. This is of particular interest in semiconductor laser dynamics, because the direct measurement of (long pieces of) time series is still an unsolved technical problem.

Specifically, we study four transitions in detail. First, we discuss a bistability arising at the locking boundary for negative detuning, which is the topic of Section 2. Second, we identify in Section 3 a region of period-three oscillations and the bifurcations bounding it. Third, we give a detailed account of bifurcations when passing a saddle-node Hopf point (marking the top of the locking range for small positive detuning) in Section 4. Finally, we identify in Section 5 the exact nature of a sudden transition to chaos as an intermittent transition by showing the associated stable and unstable manifolds.

2. Bistability at the locking boundary

As was mentioned in Section 1, diamonds in Fig. 1(a) mark the transition to locking. Full and open diamonds at negative detuning mark the boundaries of a region of bistability between the locked steady state and a periodic orbit (associated with four-wave mixing). This bistability phenomenon was observed in [7] and then it was studied numerically in [8], but the authors did not recognise the underlying bifurcation mechanism. This motivated the asymptotic analysis in [9], which revealed the existence of a torus bifurcation curve for negative detunings.

For the DFB laser considered here, this torus bifurcation appears as the grey curve T in Fig. 1(b). In fact, the bifurcation curve T was computed first, and this prompted extra measurements resulting in the identification of the open diamonds in Fig. 1(a). The measurements were performed by sweeping the injection strength up and down and detecting the transitions of the associated hysteresis loop. The two experimental spectra Fig. 2(a1) and (b1) were taken for the same values of injection strength and detuning and show the coexisting steady state and periodic solution, respectively. The theoretical spectra and the associated phase portraits are shown in Fig. 2(a2), (a3) and (b2), (b3). We remark that the sidebands around the right hand, unlocked peak of Fig. 2(b1) are the noise-induced, damped relaxation oscillation, and similar, but weaker, features appear in the spectrum of the free-running laser [5]. Note that the unlocked peak has shifted to a positive offset frequency due to the optical injection at a negative offset frequency. This frequency pushing, as opposed to the more common frequency pulling in laser injection locking, is a manifestation of the change in average carrier density due to the injected signal, and the dependence of the refractive index of the semiconductor laser on the carrier density [10]. The laser oscillation frequency and dynamic resonance frequency depend on the optical injection in a complex manner.

We now describe how the hysteresis comes about. At low injection, the laser settles down to the periodic orbit (four-wave mixing). By injecting more light, a stable equilibrium appears on the black part of SN. The two attractors coexist as shown in Fig. 2, but the equilibrium is unnoticed until the grey curve T (or the line of open diamonds)

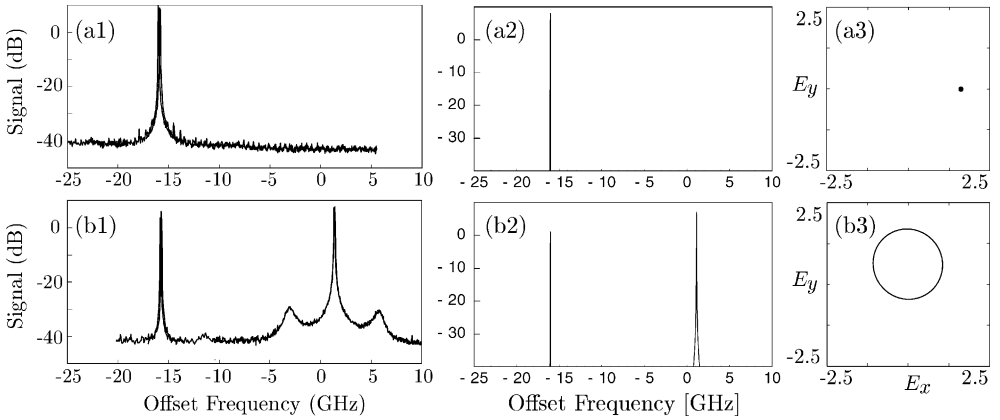

Fig. 2. Experimental spectra of the stable equilibrium (a1) and periodic orbit (b1) for $\omega = -16$ GHz and the injection field ≈ 3.5, compared with theoretical spectra of the stable equilibrium (a2) and periodic orbit (b2) for $\omega = -16$ GHz and $K = 1.7$, and the corresponding theoretical phase portraits (a3) and (b3).

is crossed. There the stable periodic orbit becomes unstable via a subcritical torus bifurcation and all trajectories converge to the stable equilibrium. When decreasing the injection strength from well inside the locking region, the stable periodic orbit appears on T and remains unnoticed until SN when it finally disappears.

3. Period-three region

Any system with complicated dynamics will have regions in parameter space in which one can find attracting periodic solutions of high period. Well-known are the regions of 2^n-periodic orbits along a period-doubling route to chaos. However, even in the ensuing region of chaos there are infinitely many windows of periodic orbits (of any multiple of the basic period). The higher the period of the orbit under consideration, the smaller the associated window of its stability. In fact, only windows of low-period orbits are likely to be detected in an experiment. A three-periodic orbit (of about three times the basic period) was recently found experimentally in an injected semiconductor laser in the parameter region near [11] and after [12] a period-doubling route to chaos.

Here we give an example of a period-three region not associated with period-doubling to chaos, but with a resonance tongue for negative detuning. It is known now that, in injected semiconductor lasers, curves of saddle-node of limit-cycle bifurcations (SL) tend to accumulate along the part of the curve of saddle-node bifurcations of equilibria (SN) for negative detunings [13–15]. In fact, in [15] it was shown that these curves SL can be regarded as 'remains' of a structure of accumulating regions of periodic orbits found in the case of a gas or a solid state laser (with $\alpha = 0$).

The region in parameter space and the period-three orbit we consider here are shown in Fig. 3. In panel (b) we show an enlargement of the bifurcation diagram from Fig. 1(b) now featuring the two extra closed curves SL^1 and SL^3 of saddle-node of limit-cycle bifurcations. The corresponding experimental diagram is shown in Fig. 3(a), where the experimentally determined region of period-three oscillations is shaded grey. An example of a spectrum in this region is shown in Fig. 3(c). The difficulty in determining the region of period-three oscillations is twofold. First, the period-three peaks need to be 'large enough' (at least 5 dB above the noise level). Second, the extra peaks need to be exactly at 1/3 intervals between the main peaks. Indeed, the period-three oscillation may be lost either by the peaks becoming too small, or by a loss of locking (that is, by a drift in frequencies). The computation of bifurcation curves was used to locate the general parameter region in which period-three orbits should exist.

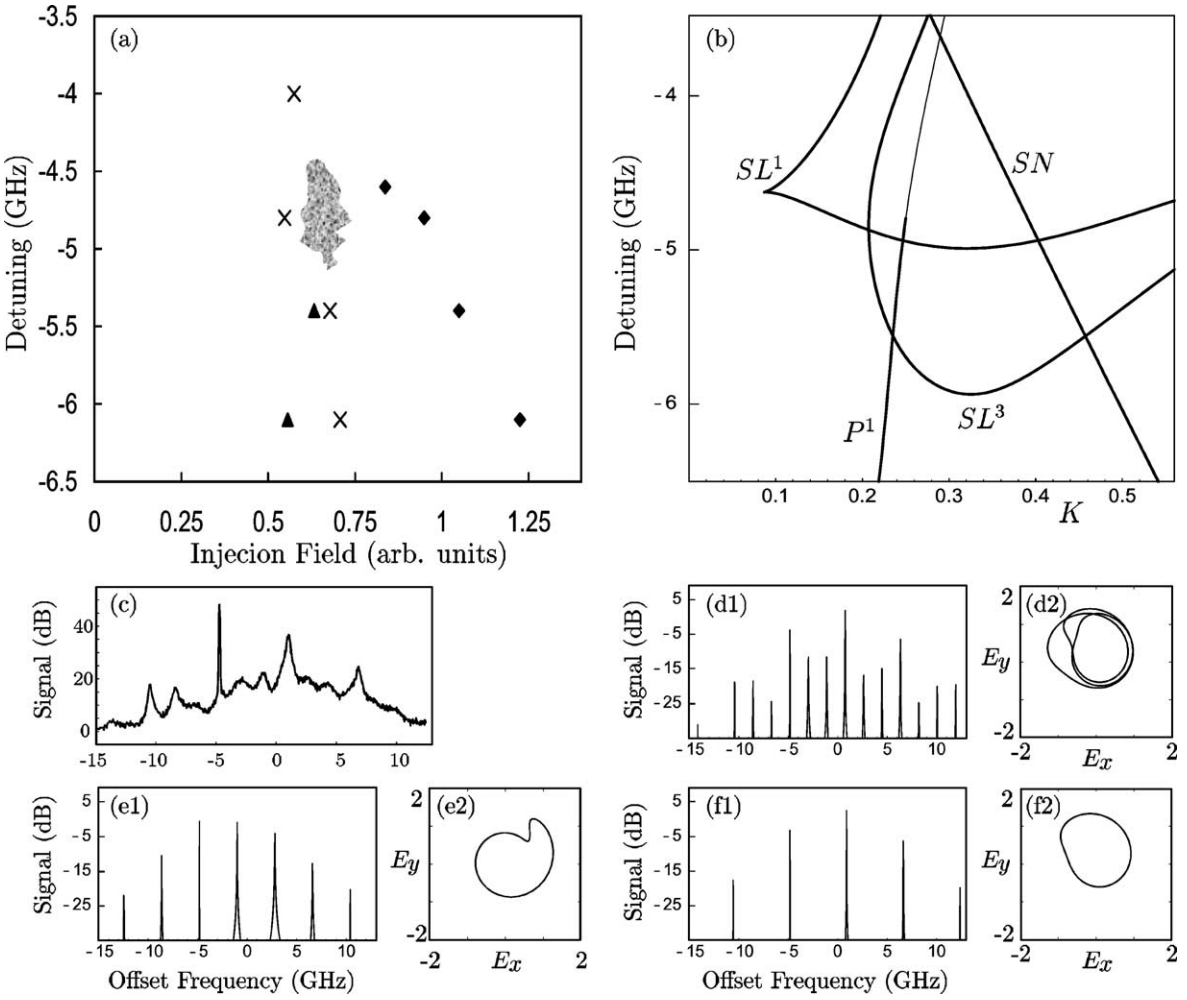

Fig. 3. Region of period-three oscillation detected experimentally, shaded grey in panel (a), together with the corresponding theoretical bifurcation diagram (b); comparison between the measured (c) and the calculated (d1) optical spectra of the period-three oscillation, as well as the optical spectra of simultaneously present period-one orbits (e1), (f1). Panels (d2)–(f2) show the associated phase portraits as projections onto the complex electric field plane. In panel (c) $\omega = -4.8$ and the injection field ≈ 0.6, and in panels (d1),(d2)–(f1),(f2) $\omega = -4.8$ and $K = 0.21$.

However, the exact region of period-three oscillations was then found experimentally by using the above criteria, without reference to the bifurcation curves.

Even at this considerably detailed and subtle level, we found very good agreement between experiment and theory. Fig. 3(d) shows the period-three orbit of Eq. (1) and the associated optical spectrum, which agrees well with the experimental spectrum in Fig. 3(c) (recall that there is no noise term in Eq. (1)). The region of period-three oscillations is bounded by a short supercritical piece of the curve SL^3. (The difference between sub- and super-critical is not indicated in Fig. 3(b).) The period-three orbit coexist with the running phase solution and with a periodic orbit born along the curve SL^1. The running phase solution is shown in Fig. 3(e). It disappears along the curve SN (the locking boundary). The orbit born along SL^1 is shown in Fig. 3(e). It appears to have a tiny basin of attraction and is already hard to find numerically.

We found theoretically that the period-three orbit, and in fact also the running phase solution, undergo further instabilities to more complicated dynamics as one moves out of the region of stable period-three dynamics. This was also found to be the case in the experiment, leading to the detection of the crosses in Fig. 3(a). The vicinity of further bifurcations made it difficult to determine the exact boundary of period-three oscillations experimentally. However, the good comparison with the theoretical bifurcation diagram added a degree of confidence in measurements that tested the limits of the experimental accuracy.

4. Transition near saddle-node Hopf point

In the stability map in Fig. 1(a) there is an important special point where the saddle-node curve SN and the Hopf curve H come together at $(K,\omega)\approx(0.1,0.15)$. This point marks the top corner of the locking region (for smaller values of K), and it is mathematically a codimension-two bifurcation called a saddle-node Hopf point, which we denote by G_1. In the bifurcation diagram in Fig. 1(b) the saddle-node Hopf point marks the transition from super- to sub-criticality of the curves SN and H. This bifurcation point is known to be the organising centre for more complicated dynamics in many different systems from applications; see, for example, [16,17] and further references therein. Specifically, in the injected laser the point G_1 received quite some attention, because several other bifurcations are associated with this point, including torus bifurcations, global bifurcations, and small regions of chaos; see Refs. [6,18,19]. (We remark that there is a second point G_2 for very large negative detuning, that moves to small negative detunings when α goes to zero [6].)

To see how the point G_1 influences the observed spectra, we fix ω to 2 GHz and increase the injection strength. In other words, we sweep directly over the point G_1 and record regions of diverse dynamics. The results are shown in Fig. 4 in direct comparison between experimental spectra, theoretical spectra and the associated phase portraits of Eq. (1).

In Fig. 4(a) the injected light is very low and we observe unlocked laser operation with the laser peak near 0 GHz being pulled slightly towards the injected peak at 2 GHz. As the amount of injected light is increased (Fig. 4(b1)), the experimental spectrum shows more peaks, forming what we call a *pedestal*. The theoretical spectrum (Fig. 4(b2)) and the associated phase portrait (Fig. 4(b3)) show that for this value of injection we are apparently dealing with complicated periodic dynamics. In fact, Fig. 4(b) indicates that the dynamics in this region appears to be a locked periodic orbit of high period on a torus. The pedestal observed in the experiment is most likely formed by many peaks of small width that come close to each other. As K is increased further, the torus breaks up into a chaotic attractor (Fig. 4(c3)) as the chaotic region inside the P^1-bubble in Fig. 1 is entered. This results in a continuous spectrum (indicative of chaotic dynamics) (Fig. 4(c2)) in good agreement with the experimental measurement (Fig. 4(c1)). Upon increasing the injection strength (Fig. 4(d)) the spectrum broadens considerably. This can be explained by a change of the chaotic attractor, which evolves from a slightly broken torus (Fig. 4(c)) into fully developed chaos (Fig. 4(d3)).

Increasing K even further, the other boundary of the chaotic region is approached. The spectrum is still chaotic but strong periodic components start to appear (Fig. 4(e1)) as the chaotic attractor becomes smaller in size (Fig. 4(e3)). Very close to this boundary the periodic component in the spectrum becomes more distinct (Fig. 4(f1)) but each peak has a pedestal. While this might still indicate chaotic dynamics, our calculations show that this type of spectrum most likely represents a complicated periodic oscillation: the pedestal appears to be formed by several low peaks accumulating onto each of the high peaks (Fig. 4(f2)). After the chaotic region is left, the laser produces period-one self-pulsations (Fig. 4(g)). Increasing the injection strength even more, the big uppermost period doubling bubble in Fig. 1 is approached. In the experiment we pass just below the period doubling transition (triangles in Fig. 1(a)) but, due to the influence of noise, the laser 'feels' the closeness of this bifurcation, and it shows low peaks at half frequencies (Fig. 4(h1)).

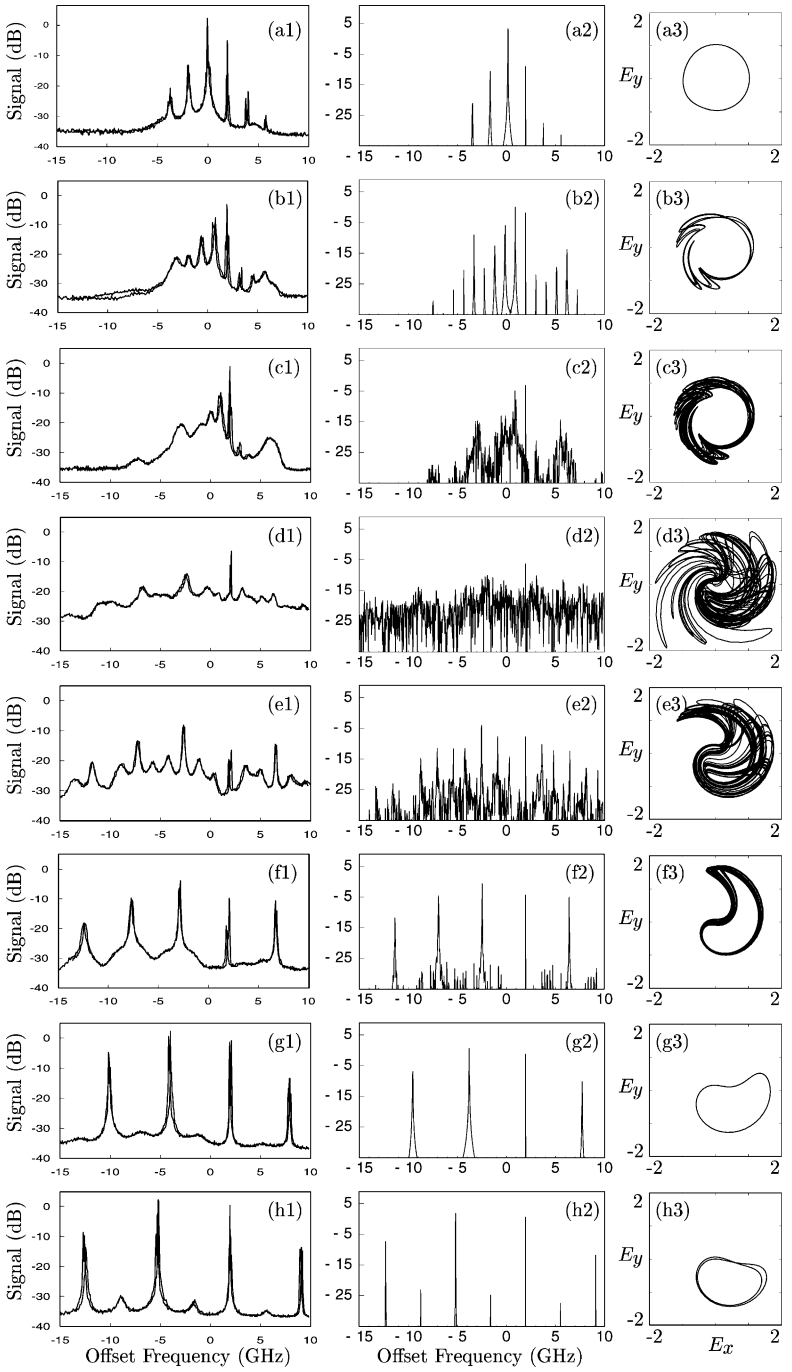

Fig. 4. Experimental spectra (first column), theoretical spectra (second column), and corresponding theoretical phase portraits (third column) for the transition at $\omega = 2$ GHz. From (a1) to (h1) the experimental injection field takes the values 0.15, 0.31, 0.37, 0.71, 1.22, 1.32, 1.60, and 2.29; from (a2),(a3) to (h2),(h3) K takes the values 0.06, 0.13, 0.14, 0.26, 0.35, 0.37, 0.45, and 0.82.

5. Intermittent transition to chaos

Encouraged by the very good agreement we found for different types of periodic dynamics as well as for the more complicated bifurcation transition near the saddle-node Hopf point, we decided to go even further and try to measure a sudden chaotic transition. As was reported in Ref. [20] certain regions of chaotic dynamics can be entered or exited via different bifurcation scenarios depending on the chosen path in the (K,ω)-plane. This is also true for a region of chaos around $(K,\omega)\approx(0.3,2.0)$, inside the small island bounded by P^1; see Fig. 1. One route to chaos here is via successive period-doublings (of which P^1 and the triangles is the first). However, the upper part of the curve P^1 is subcritical, so that there must be a different transition out of chaos when, say, ω is increased. This is also reflected in the experimental stability diagram in Fig. 1(a) where crosses appear, instead of triangles.

This route into and out of chaos is an intermittent chaotic transition as shown in Fig. 5; see [20] for more details on the theory. Panels (a1)–(c1) show experimental optical spectra across this transition, where each plotted panel consists of two overlaid measurements. Initially, the laser produces chaotic output (Fig. 5(a1)) with a quite broad spectrum. The sharp peak at 3 GHz is the injection frequency, and no other periodic components are clearly distinguishable. At the moment of bifurcation (to within the experimental accuracy) one notices clear periodic features arising out of the broad chaotic background of the spectrum (Fig. 5(b1)). Furthermore, the two overlaid spectra separate due to the increased sensitivity of the system to parameter fluctuations near the bifurcation. Changing the detuning only slightly results in an abrupt change to periodic oscillations (Fig. 5(c1)). We stress that there is no hysteresis in this transition.

To explain what is going on we computed the corresponding attractors of Eq. (1) in the Poincaré section $\{n=0\}$ in Fig. 5(a3)–(c3) and their spectra in (a2)–(c2). These spectra show exactly the same qualitative and quantitative features as the experimental optical spectra (again taking into account that Eq. (1) is a deterministic system without

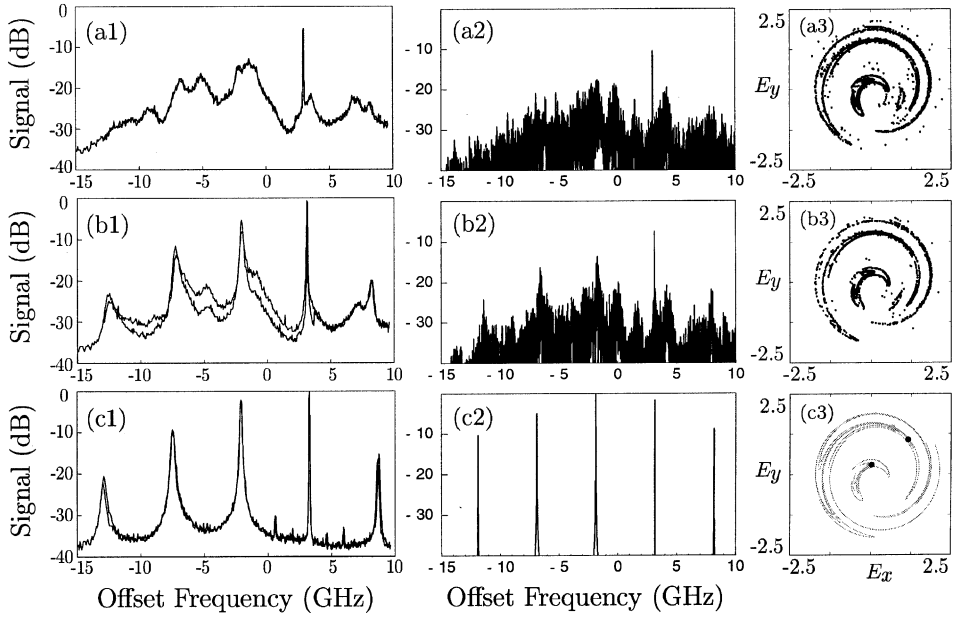

Fig. 5. An intermittent transition shown as experimental spectra (first column), theoretical spectra (second column), and theoretical Poincaré section $\{n=0\}$ (third column). From (a1) to (c1) ω takes the values 3, 3.13, and 3.2 GHz and the injection field was $\approx$1. From (a2),(a3) to (c2),(c3) ω takes the values 3, 3.11, and 3.15 GHz and $K=0.31$.

noise). The plots in the Poincaré plane reveal the nature of the transition: a saddle-node bifurcation of limit cycles takes place *on* a chaotic attractor. Indeed we see the chaotic attractor as a fractal set in Fig. 5(a3) and (b3). Then suddenly, it is gone and we see distinct points in the Poincaré section: the two black dots correspond to an attracting periodic orbit and the two grey dots to a saddle periodic orbit of Eq. (1). Also plotted in grey are the unstable manifolds of the saddle points of the Poincaré map. Notice that these manifolds resemble the chaotic attractor, leading to chaotic transients before the system settles down to periodic output.

This shows conclusively that we are dealing with an intermittent transition into or out of chaos. The intermittency occurs in the chaotic region just before the transition: the trajectory stays near where the saddle-node will appear for long and irregular periods of time. This leads to clearly discernible periodic intervals in the overall chaotic dynamics. The intervals become longer and longer the closer the system is to the actual saddle-node bifurcation of limit cycles. This manifests itself in the spectrum as an increasing periodic component, the narrow peaks we observe in Fig. 5(b). We actually computed the curve SL of saddle-node of limit cycle bifurcation and it agrees very well with the crosses at the upper boundary of this region of chaos; see Fig. 1.

6. Conclusions

We demonstrated very good qualitative and quantitative agreement between theory and experiment of entire bifurcation transitions in an optically injected semiconductor laser. This shows that the agreement between the experimental stability map and the bifurcation diagram of the rate equations is matched by the corresponding phase portraits to such a degree that their spectra can directly and quantitatively be compared with the optical spectra measured in the experiment. This allows us to determine the exact nature of even complicated dynamics and their bifurcations in a system where time traces of sufficient length cannot be measured at present because of the fast time scales involved.

From the dynamical systems theory point of view, the injected semiconductor laser belongs to the best examples of agreement between a low-dimensional ODE model and experiments on the actual physical device.

Acknowledgements

The research of S.W. was supported by the Foundation for Fundamental Research on Matter (FOM), which is financially supported by the Netherlands Organisation for Scientific Research (NWO). The work of T.B.S. was supported, in part, by the U.S. Army Research Office under contract DAAG-55-98-C-0038. The research of B.K. was supported by an ARF grant from the UK's Engineering and Physical Sciences Research Council.

References

[1] S. Strogatz, Nonlinear Dynamics and Chaos, Perseus Publishing, 1994.
[2] B. Krauskopf, D. Lenstra (Eds.), Fundamental Issues of Nonlinear Laser Dynamics, AIP Conference Proceedings, vol. 548, 2000.
[3] S. Wieczorek, The dynamical complexity of optically injected semiconductor lasers, Ph.D thesis, Vrije Universiteit Amsterdam, 2002.
[4] S. Wieczorek, T.B. Simpson, B. Krauskopf, D. Lenstra, Phys. Rev. E 65 (045207(R)) (2002) 1.
[5] T.B. Simpson, Mapping the nonlinear dynamics of a distributed feedback semiconductor laser subject to external optical injection, Opt. Commun. 215 (2003) 135–151.
[6] S. Wieczorek, B. Krauskopf, D. Lenstra, Opt. Commun. 4172 (1–6) (1999) 279.
[7] R. Hui, A. D'Ottavi, A. Mecozzi, P. Spano, IEEE J. Quantum Electron. 27 (1991) 1688.
[8] J.M. Liu, H.F. Chen, X.J. Meng, T.B. Simpson, IEEE Photon. Technol. Lett. 9 (1997) 1325.
[9] V. Kovanis, T. Erneux, A. Gavrielides, Opt. Commun. 159 (1999) 177.
[10] T.B. Simpson, J.M. Liu, K.F. Huang, K. Tai, Quant. Semiclass. Opt. 9 (5) (1997) 765.
[11] A. Gavrielides, V. Kovanis, M. Nizette, T. Erneux, T.B. Simpson, J. Opt. B: Quant. Semiclass. Opt. 4 (2002) 20.
[12] S. Eriksson, Å.M. Lindberg, Opt. Lett. 26 (2001) 142.
[13] S. Wieczorek, B. Krauskopf, D. Lenstra, Opt. Commun. 183 (1–4) (2000) 215.
[14] A. Gavrielides, V. Kovanis, P.M. Varangis, T. Erneux, G. Lythe, Quant. Semiclass. Opt. 9 (5) (1997) 785.
[15] B. Krauskopf, S. Wieczorek, Physica D 173 (2002) 97.

[16] J. Guckenheimer, P. Holmes, Nonlinear Oscillations, Dynamical Systems and Bifurcations of Vector Fields, Springer, Berlin, 1986 (second printing).
[17] Yu.A. Kuznetsov, Elements of Applied Bifurcation Theory, Applied Mathematical Sciences, vol. 112, Springer, Berlin, 1995.
[18] C. Mayol, M.A. Natiello, M.G. Zimmermann, Int. J. Bifur. Chaos 11 (2001) 2587.
[19] M. Nizette, T. Erneux, A. Gavrielides, V. Kovanis, Physica D 161 (2002) 220.
[20] S. Wieczorek, B. Krauskopf, D. Lenstra, Phys. Rev. E 64 (056204) (2001) 1.